

1 **Inland lake temperature initialization via coupled cycling with atmospheric data**
2 **assimilation**

3
4 Stanley G. Benjamin¹, Tatiana G. Smirnova^{2,1}, Eric P. James^{2,1}, Eric J. Anderson³,
5 Ayumi Fujisaki-Manome^{4,5}, John G.W. Kelley⁶, Greg E. Mann⁷, Andrew D. Gronewold⁵
6 Philip Chu⁸, Sean G.T. Kelley⁹

7
8 ¹NOAA Global Systems Laboratory, Boulder, CO 80305 USA

9 ²Cooperative Institute for Research in Environmental Science (CIRES), University of
10 Colorado, Boulder, CO 80303 USA

11 ³Civil and Engineering Department, Colorado School of Mines, Golden, CO USA

12 ⁴Cooperative Institute for Great Lakes Research (CIGLR), University of Michigan, Ann
13 Arbor, MI USA

14 ⁵University of Michigan, Ann Arbor, MI USA

15 ⁶NOAA National Ocean Service, Coast Survey Development Laboratory, Durham,
16 NH 03824 USA

17 ⁷NOAA National Weather Service, White Lake, MI, USA

18 ⁸NOAA Great Lakes Environmental Research Laboratory, Ann Arbor, MI, USA

19 ⁹University of Massachusetts, Department of Mathematics and Statistics,
20 Amherst, MA, USA

21
22 *Correspondence to:* Tatiana Smirnova (tanya.smirnova@noaa.gov)

23
24 8 Dec 2021 - submitted to Geoscientific Model Development (GMD)

25 https://gmd.copernicus.org/articles/special_issue1114.html

26 Special issue I Modelling inland waters in a changing climate (GMD/ESD/TC inter-
27 journal SI).

28 - Resubmitted with editorial changes – 21 Jan 2022, 21 June 2022, 28 July 2022

29
30 **Abstract.** Application of lake models coupled within earth-system prediction models,
31 especially for predictions from days to weeks, requires accurate initialization of lake
32 temperatures. Commonly used methods to initialize lake temperatures include
33 interpolation of global SST analyses to inland lakes, daily satellite-based observations
34 or model-based re-analyses. However, each of these methods have limitations in
35 capturing the temporal characteristics of lake temperatures (e.g., effects of anomalously
36 warm or cold weather) for all lakes within a geographic region, and/or during extended
37 cloudy periods. An alternative lake initialization method was developed which uses 2-
38 way coupled cycling of a small-lake model within an hourly data assimilation system of a
39 weather prediction model. The lake model simulated lake temperatures were
40 compared with other estimates from satellite and in-situ observations and interpolated-
41 SST data for a multi-month period in 2021. The lake cycling initialization, now applied
42 to two operational US NOAA weather models, was found to decrease errors in lake
43 surface temperature from as much as 5-10 K vs. interpolated-SST data to about 1-2 K
44 compared to available in-situ and satellite observations.

45
46
47
48
49
50
51
52
53
54
55
56
57
58
59
60
61
62
63
64
65
66
67
68
69
70
71
72
73
74
75
76
77
78
79
80
81
82
83
84
85
86
87

Short summary

Application of 1-d lake models coupled within earth-system prediction models will improve accuracy but requires accurate initialization of lake temperatures. Here, we describe a lake initialization method by coupled cycling within a weather prediction model to constrain lake temperature evolution. We compare these lake temperature values with other estimates and found much reduced errors (down to 1-2 K). The lake cycling initialization is now applied to two operational US NOAA weather models.

1 Introduction

Inclusion of lake representation into numerical weather prediction (NWP) models has become increasingly necessary to further improve representation of atmosphere-surface fluxes of heat and moisture as model grid resolution becomes finer. Representation of lake physics to provide time-varying lake surface properties (e.g., Subin et al, 2012) is essential to improve fluxes of heat, moisture and momentum between the surface and atmosphere (Hostetler et al, 1993, Thiery et al, 2014). Lake representation is part of the overall surface treatment including land-surface models (LSMs) necessary to accurately model the evolution of the planetary boundary layer in the atmosphere. Lakes are estimated to cover 3.7% of the global non-glaciated land area (Verpoorter et al, 2014), and they significantly moderate sensible heat and moisture fluxes from this ‘land’ (i.e., non-ocean) area. Water impoundments (reservoirs) that used to account for about 6% of these ‘lake’ areas (Downing et al, 2006) have recently increased to 9% (Vanderkelen et al, 2021). Initial conditions for both land and lake surface are an important consideration due to far larger thermal inertia for soil or water than for air. Consequently, incorrect soil or lake initial conditions can result in erroneous heat and moisture fluxes that may persist for days and even weeks (e.g., Dirmeyer et al, 2018). This potential source of error in fluxes is more pronounced for lake areas with far larger thermal inertia and heat storage than even saturated soils.

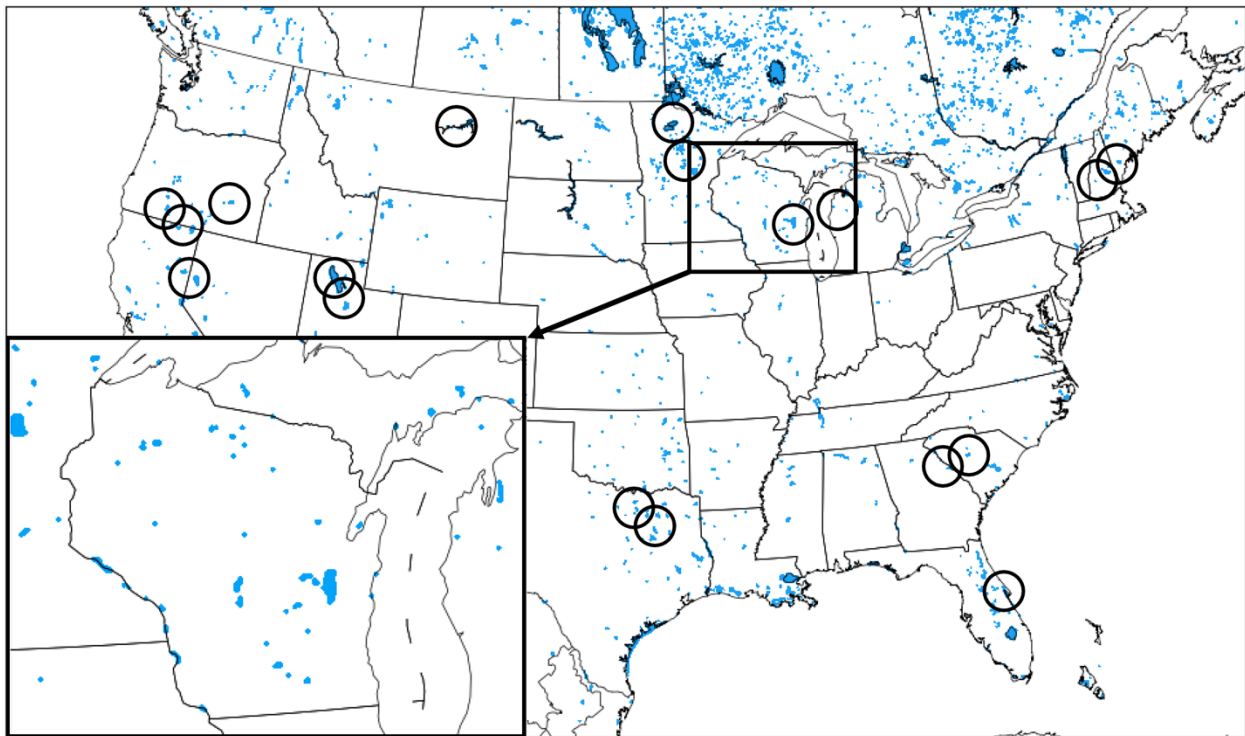
In operational US NOAA weather prediction models (global and regional) up to this point, daily sea-surface temperature (SST) analyses have been used to specify the surface water temperatures for even small inland lakes. Inland lake temperatures in North America have been obtained by the interpolation of SST values from the ocean and the Laurentian Great Lakes. An alternative is to incorporate one-dimensional (1-d) lake models within NWP models and use a continuous lake simulation forced by atmospheric conditions updated regularly by new atmospheric observations to obtain realistic lake water temperatures (e.g., “cycling”). This cycling to initialize small lakes in NOAA operational regional weather prediction models complements loose coupling with a 3-d hydrodynamical lake model for the Laurentian Great Lakes as described elsewhere in Fujisaki-Manome et al 2020.

88 Lake representation (via one-dimensional (1-d) models, as in LSMs) within NWP
89 models is beneficial by providing a first-order accurate lagged effect of the seasonal
90 variation in temperature, with lake water remaining colder than nearby land in spring
91 and warmer in autumn. The outcomes are desirable, as described by Balsamo et al
92 (2012), for instance by accurately representing increased evaporative fluxes in the fall.
93 Thus, use of a 1-d lake model has the potential to improve over land representation by
94 capturing this slower seasonal response.

95
96 However, lake temperature initialization from SST (e.g., Mallard et al, 2015) can
97 exaggerate this seasonal slower response. Shallow lakes warm more slowly in spring
98 than surrounding land, but more quickly than nearby deeper lakes. Even in summer, it
99 will take at least 1-2 weeks for cycled 1-d models to adjust from values interpolated from
100 deeper-lake temperatures to become more realistic for shallow lakes. Therefore, lake
101 temperature initialization becomes the most important factor to accurately simulate
102 sensible and latent heat fluxes from lakes for short to medium-range NWP, more so
103 than the use of the lake model itself. One option to solve the lake initialization problem
104 is to use a model-based climatology for seasonal variation of lake temperatures
105 (Balsamo et al (2012) and Balsamo (2013), ECMWF) using a 1-d lake model forced by
106 reanalysis data. The 1-d lake model used by ECMWF for this method is the 2-layer
107 FLake (Freshwater Lake Model) model (Mironov et al, 2010, Balsamo et al, 2012,
108 Boussetta et al, 2021) and also implemented into their Integrated Forecast System (IFS)
109 in 2015. A similar technique was applied by Mironov et al (2010) using FLake for the
110 COSMO model. Kourzeneva et al (2012a) describe application of 20-year reanalysis
111 data to create a global lake climatology dataset using FLake. This technique avoids a
112 new spin-up with each new run, but cannot capture unique weather regime variations in
113 a given region and time. The UK Met Office uses satellite data to update their lake
114 surface water temperatures using the previous day values as a background (Fiedler et
115 al, 2014). Another option to solve the lake initialization problem, described here, is lake
116 temperature evolution, referred to as “lake cycling”, with the ongoing 1-d lake prediction
117 within an NWP model, a cost-free option if the atmospheric conditions are relatively
118 accurate.

119
120 Data assimilation for land-surface fields (e.g., soil temperature, soil moisture, snow
121 cover, snow water equivalent, snow temperature) has been very beneficial for improved
122 short-range weather prediction accuracy (e.g., Balsamo and Mahfouf, 2020, Muñoz-
123 Sabater et al, 2019, Benjamin et al, 2022, others), but lake temperature has not been a
124 part of this surface data assimilation. In December 2020, the two NOAA hourly updated
125 weather models, the 13-km Rapid Refresh (RAP) and 3-km High-Resolution Rapid
126 Refresh (HRRR) implemented an interactive small-lake multi-layer 1-d lake model, the
127 first NOAA weather models to do so. The lake coverage for the HRRR model is shown
128 in Fig. 1 (RAP model lake coverage not shown). The HRRR and RAP weather models
129 are coupled with the 10-layer Community Land Model (CLM) version 4.5 lake model,
130 (Subin et al, 2012, Mallard et al, 2015), an option within the community Weather
131 Research and Forecast model (WRF, Skamarock et al, 2019). The CLM lake model is a

132 1-d thermal diffusion model allowing 2-way coupling with the atmosphere. Virtually no
133 additional computational cost (<0.1 %) was added by use of the CLM lake model within
134 the HRRR model. To initialize small-lake temperatures in the RAP and HRRR, all lake
135 variables have been evolving (e.g., “lake cycling”) since summer 2018 depending on the
136 cycled atmospheric conditions and the lake model physics as discussed in section 4.
137 This cycling is similar to the land-surface cycling in HRRR and RAP as described by
138 Benjamin et al (2022). The 1-d lake model cannot represent 3-d hydrodynamical
139 processes in larger bodies of water. Thus, a second major improvement in 2020 with
140 lake representation in the NOAA 3-km HRRR model occurred with the implementation
141 of lagged data coupling with the 3-d hydrodynamic-ice model for the much larger
142 Laurentian Great Lakes as described by Fujisaki-Manome et al (2020). These new
143 improved lake treatments are in the newer HRRR version 4 (HRRRv4) replacing the
144 previous HRRRv3 (differences described in Dowell et al, 2022; hereafter D22).
145
146



147
148 *Fig. 1. Small-lake areas for the 3-km HRRR domain using the MODIS 0.15” resolution*
149 *data for land/water and lake information. Only small-lake areas treated in HRRR by the*
150 *1-d CLM lake model are shown. A zoomed-in insert for HRRR small-lake coverage in*
151 *the vicinity of the state of Wisconsin is shown in the lower left. Out of the 1,900,000*
152 *grid points in this HRRR CONUS domain, 12,305 of them (~0.6%) are for small lakes*
153 *(excluding the 5 Laurentian Great Lakes treated by separate coupling as described in*
154 *text). Lakes circled in black were related to problem reports from US National Weather*
155 *Service Forecast Offices on nearby deficient 2 m air temperature or dewpoint forecasts*
156 *in NOAA hourly updated models as discussed in section 2.*
157

158 Here, we describe the design and results of a unique approach to inland-small-lake
159 initialization by cycling with hourly updating of atmospheric conditions (clouds/radiation,
160 near-surface temperature/moisture/winds). This lake initialization via cycling is an
161 important component of earth-system coupled modeling for effective NWP, with goals to
162 improve prediction of 2-m (air) temperature and moisture, cloud, boundary-layer
163 conditions, and precipitation for situational awareness enabling short-range decision
164 making (e.g., aviation, severe weather, hydrology, energy).

165

166 **2 The Lake Initialization Problem**

167

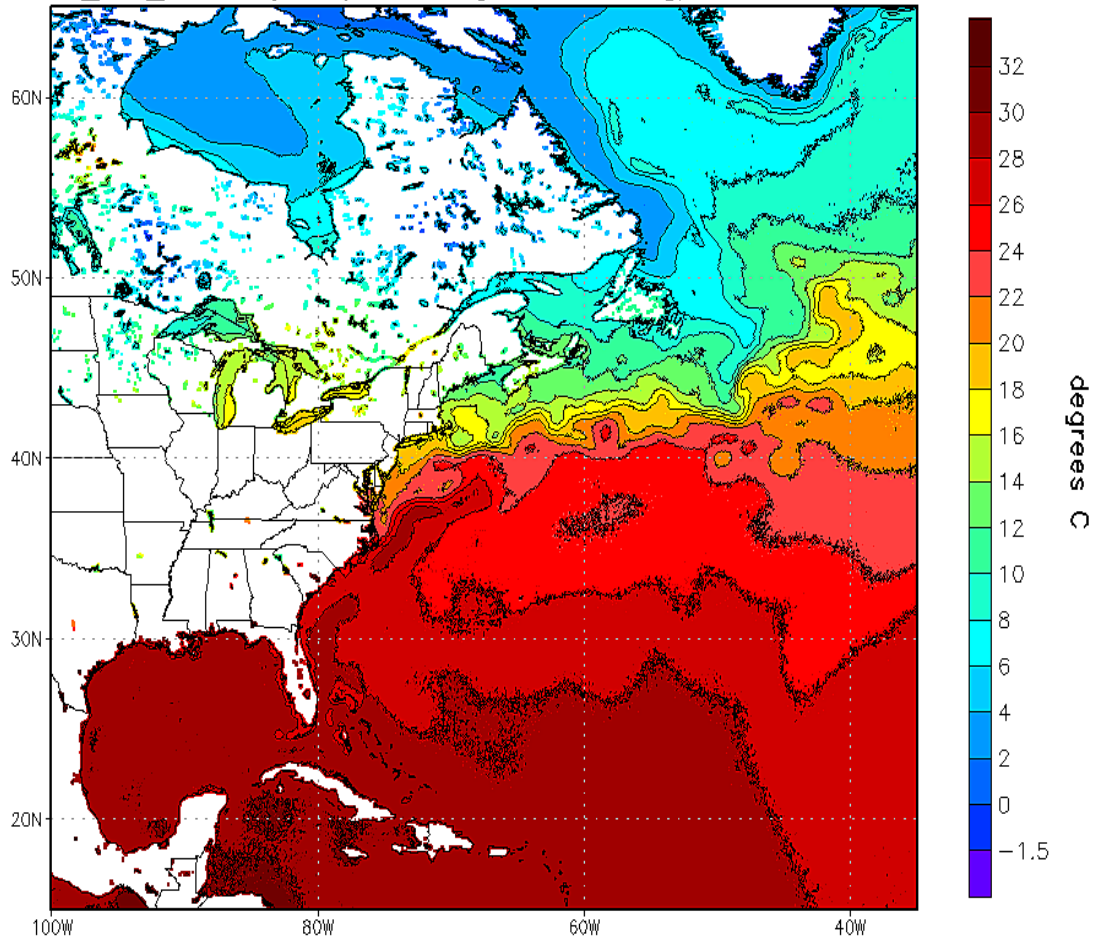
168 For the NOAA hourly updated mesoscale models, used frequently for short-range
169 weather prediction, poor 2 m air temperature and/or dewpoint forecasts have been
170 reported intermittently during 2004-2019 by the US National Weather Service (NWS) in
171 the vicinity of inland lakes (Fig. 1). These hourly updated models included the Rapid
172 Update Cycle (RUC, Benjamin et al, 2004) with horizontal grid spacing decreasing from
173 40-km to 20-km to 13-km (Benjamin et al, 2010), succeeded by the 13-km RAP and 3-
174 km HRRR (Benjamin et al, 2016, D22, James et al, 2022 (J22)). Many of these
175 reported systematic deficiencies from the US NWS were for the 2.5-km NOAA Real-
176 Time Mesoscale Analysis (RTMA, Pondeva et al. 2011), using 1-h forecasts from the 3-
177 km HRRR as a background. The most common report was too-low 2 m air temperatures
178 near inland lakes in late spring and summer. At times, spurious prediction of fog
179 formation was also noted on or near small lakes due to too-cold lake temperatures and
180 erroneous heat and moisture fluxes into the atmosphere.

181

182 Further investigation revealed the water temperatures for small lakes used in NOAA
183 weather models were assigned via horizontal interpolation from larger, deeper bodies of
184 water (with available AVHRR data) in the design for the NOAA real-time gridded SST
185 analysis (RTG_SST_HR, Gemmill et al, 2007). An example of the analysis is shown in
186 Fig. 2. Temperature for the larger, deeper water areas has a lesser and more lagged
187 seasonal variation than the smaller, shallower lake areas due to their large heat storage
188 capacity. Therefore, use of the NOAA SST fields for lake temperatures resulted in
189 generally too-low values through spring and summer, and even into autumn. In
190 situations with atmospheric cold outbreaks in the autumn, shallow lake temperatures
191 quickly decrease (as reflected with lake cycling) and SST-based estimated lake
192 temperatures were too high. This behavior was consistent with the HRRR and RTMA
193 deficiencies noted by forecasters. In February 2020, NOAA changed from the
194 RTG_SST_HR to a Near-Surface Sea Temperature (NSST, see NWS, 2020) for SSTs,
195 but using the same horizontal interpolation method to estimate small-lake temperatures
196 resulting in the same temperature biases for small lakes.

197

RTG_SST_HR Analysis (0.083 deg X 0.083 deg) for 09 Oct 2019

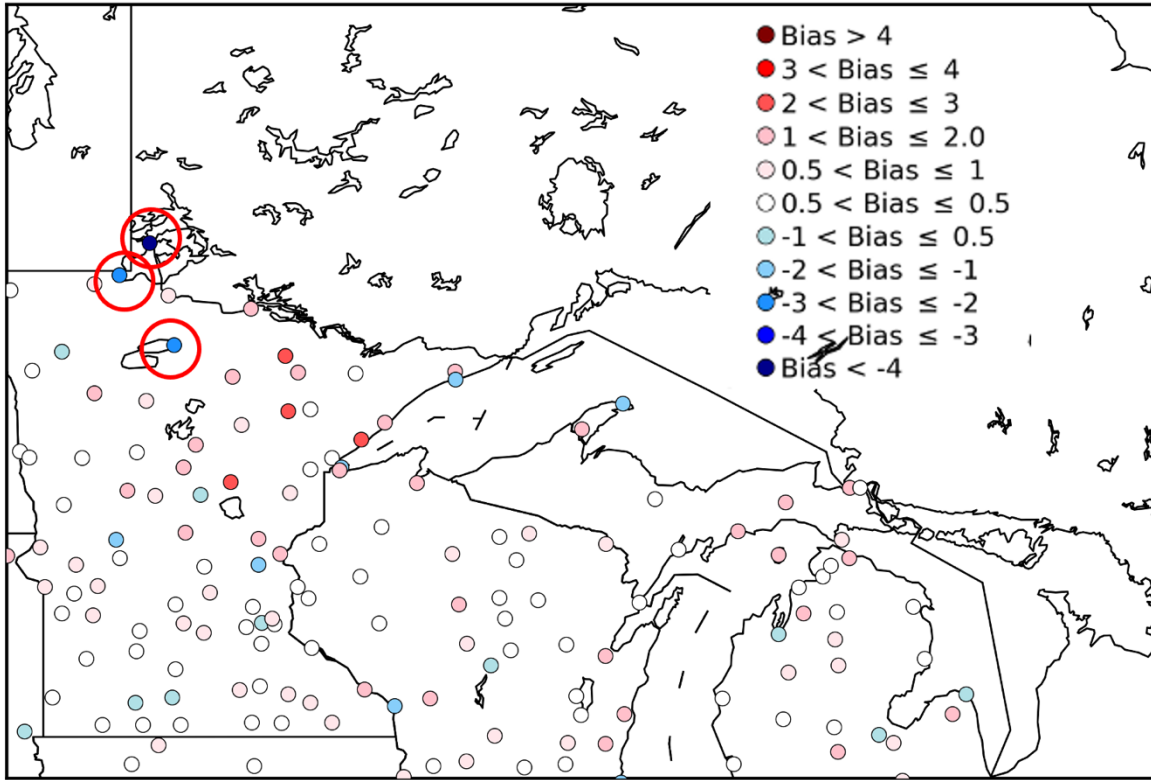


198
199

200 *Fig. 2. An example of small-lake temperatures spatially interpolated from deeper-water*
201 *temperature data in the NOAA SST analysis (Gemmill et al, 2007). For 9 October*
202 *2019, provided by NOAA National Weather Service.*

203

204 Hamill (2020), in a comparison benchmarking a statistical method for 2 m temperature
205 (at 00 UTC), showed the same problem with large summer temperature biases from the
206 HRRRv3 1-h forecasts in August 2018 especially in the vicinity of lakes (his Figs. 10,
207 11). His results are shown in Fig. 3, with three stations showing coldest biases (at 00
208 UTC) greater than 2 K (circled in red), all adjacent to lakes. In Fig. 3, these circled
209 stations, from north to south, are KFGN (Flag Island on Lake of the Woods; > 3 K cold
210 bias), KRRT - Warroad, MN (west of Lake of the Woods), and KVVU – Waskish, MN
211 (east of Red Lake)). The overall warm or cold biases are generally < 2 K, but these
212 stations adjacent to lakes are outliers, consistent with introduction of cold-biased lake
213 temperatures through the NSST.



214
 215 *Figure 3. 2 m temperature biases for 1-h HRRR forecasts valid at 00 UTC in August*
 216 *2018 (from HRRRv3, before introduction of lake cycling and using NSST estimates*
 217 *instead. HRRR versions and dates are listed in D22.). Stations with low bias < -2 K are*
 218 *circled in red. (Credit and thanks to Thomas Hamill, providing a regional version of his*
 219 *Fig. 10b in Hamill, 2020).*

220
 221

222 With its 3 km grid spacing, the HRRR model can resolve many inland lakes (Fig. 1).
 223 Specification of surface temperatures for these small lakes using the horizontal
 224 interpolation from the NOAA SST fields was problematic being determined by
 225 interpolation from large lake and ocean temperatures.

226

227 In summary, errors in specified lake temperatures (as well as ice cover and
 228 concentration) due to spatial interpolation from oceans and larger lakes can lead to
 229 degraded atmospheric predictions in the vicinity of lakes. For small lakes, poor short-
 230 range 2 m temperature (T) and 2 m dew point temperature (T_d) forecasts were noted in
 231 vicinity of lakes, especially from spring through summer and into autumn. Specifically,
 232 fluxes from lakes were often poorly estimated due to inaccurate lake temperature fields.

233

234 **3 Lake model for coupling with NOAA regional atmospheric models**

235

236 To complement the now-commonplace (in NWP models) coupling with land-surface
 237 models (LSMs) to improve fluxes into the atmosphere, a multi-level 1-d lake model was

238 implemented within the operational 3-km HRRRv4 and 13-km RAP weather models in
239 December 2020, an extension to atmosphere-surface coupling. An effective lake
240 initialization is a necessary complement for the lake model coupling, as described in
241 section 4. Different earth-system coupling processes represented in the HRRR and
242 RAP models are described in Table 1, including land, snow, ice, and smoke. The
243 Community Land Model (CLM) lake model (same in versions 4.5 and 5.0) was added
244 for smaller lakes as an option in the WRF model version 3.6 (Mallard et al, 2015). The
245 CLM lake model is described in more detail below with its configuration for the NOAA
246 HRRRv4 and RAP weather models. A detailed description of the physical processes
247 (cloud microphysics, turbulent exchange, land-surface, etc.) in the HRRR and RAP
248 models are described by D22 and Benjamin et al (2016).

Component	Prognostic variables	Layers (below surface except for smoke)	Year introduced for experimental cycling	Year intro for NCEP	Data assimilation	Other information, references
Soil	Temp, moisture	9	1996 (6 levels until 2012)	1998 (6 levels until 2014)	Cycling, atmos-to-soil coupled DA	Moderately coupled DA (Benjamin et al 2022)
Snow	Water equiv, snow depth, temp	2	1997	1998	Cycling, atmos-to-snow DA for temp, trim/build from sat for cover	Moderately coupled DA. Subgrid fraction intro 2020
Ice	Temp	9	2010 (6 levels until 2012)	2012 (6 levels until 2014)	Cycling, atmos-to-surface coupled DA	Subgrid fraction intro 2018
Smoke	Smoke mixing ratio	50 atmos layers	2016	2020	Cycling, fire rad power from sat	No direct DA, only cycling
Small lakes	Temp, ice fraction, mixing	10	2018	2020	Cycling	No direct DA, only cycling
Large lakes (Great Lakes)	Temp, ice fraction, mixing	FVCOM levels	2018	2020	Independent	FVCOM driven by HRRR wind, rad, temp, 6h lag (Fujisaki-Manome et al 2020)

249 *Table 1. Earth-system coupling added to NOAA regional models (HRRR, RAP, RUC*
250 *(pre-2012)).*

251
252 An additional improvement in lake-atmosphere coupling in NOAA weather models for
253 large lakes (>15,000 km²) was recently introduced, a coupling between the NOAA
254 HRRR model using predicted lake temperatures and ice concentration fields from the
255 NOAA GLERL/NOS 3-dimensional hydrodynamic-ice model run in real time over the
256 Laurentian Great Lakes, as described by Fujisaki-Manome et al (2020). This
257 hydrodynamic-ice model is based on the Finite Volume Community Ocean Model
258 (FVCOM, Chen et al., 2006, 2013) coupled with the unstructured grid version of Los
259 Alamos Sea Ice Model (CICE; Gao et al., 2011) and is applied to the NOAA Great
260 Lakes Operational Forecast System (GLOFS, Anderson et al., 2018). This time-lagged
261 data coupling (alternate applications of HRRR atmospheric forcing and FVCOM-CICE
262 lake forcing about 6-12 h in advance) was incorporated to improve lake-effect snow
263 (LES) predictions in winter but has also been found to improve near-lake atmospheric
264 predictions year-round especially for upwelling events in the warm season. The use of
265 FVCOM-CICE to specify lake temperatures addresses previous errors in SST from
266 relatively fast changes in lake temperatures due to cold air outbreaks or upwelling

267 events. These changes sometimes escape AVHRR-derived SST detection due to multi-
 268 day cloud obscuration.
 269

Small lake size (grid points)	# Lakes	% of # of small lakes	% of small lake surface coverage	Avg depth (m)	Surface area of lakes (km ²)	Volume of lakes (km ³)
1 grid point (3kmx3km)	917	49%	7%	13	8,812	115
2 (~20 km ²)	323	17%	5%	12	6,208	76
3	155	8%	4%	11	4,468	49
4-5	157	8%	6%	14	6,746	97
6-10 (~100 km ²)	155	8%	10%	14	11,570	162
11-100 (~1000 km ²)	141	7%	30%	21	35,518	769
>100	16	<1%	38%	14	44,926	614
All	1864	100%	100%		118,248	1,882

270 *Table 2. Characteristics of small lakes (not including the five Laurentian Great Lakes)*
 271 *resolved in the 3-km HRRRv4 CONUS domain over the lower 48 United States and*
 272 *adjacent areas of Canada and Mexico. Grid points were assigned as having a lake land*
 273 *use for points with at least 50% lake representation from the higher-resolution 15"*
 274 *MODIS land-use data.*

275
 276

Laurentian Great Lakes	Surface area of lakes (km²)	Volume of lakes (km³)
Superior	82,100	12,000
Michigan	57,800	4,920
Huron	59,600	3,540
Erie	25,670	484
Ontario	19,010	1,640

277
 278 *Table 3. Characteristics of the five Laurentian Great Lakes (surface area, volume)*
 279 *(Hunter et al 2015).*

280

281 3.1 CLM lake model applied to HRRR for smaller inland lakes

282
283 Subin et al (2012) describe the 1-d CLM lake model as applied within the Community
284 Earth System Model (CESM) as a component of the overall CESM CLM (Lawrence et al
285 2019). Gu et al (2015) describe the introduction of the CLM lake model into the WRF
286 model and initial experiments using its 1-d solution for both Lakes Superior (average
287 depth of 147 m) and Erie (average depth of 19 m). The CLM lake model divides the
288 vertical lake profile into 10 layers driven by wind-driven eddies. The atmospheric inputs
289 into the model are temperature, water vapor, horizontal wind components from the
290 lowest atmospheric level and short-wave and longwave radiative fluxes (from the HRRR
291 model in this application). The CLM lake model then provides latent heat and sensible
292 heat fluxes back to the HRRR. The CLM lake model is called every 20 s within the
293 HRRR model. The CLM lake model was configured with the top layer fixed to a 10-cm
294 thickness (Gu et al 2015) and with the rest of the lake depth divided evenly into the
295 other 9 layers. Energy transfer (heat and kinetic energy) occurs between lake layers via
296 eddy and molecular diffusion as a function of the vertical temperature gradient. The
297 version of the CLM lake model used for HRRRv4 and RAP was introduced with CLM
298 version 4.5 and continues without change in CLM version 5 (Lawrence et al, 2019). The
299 CLM lake model also uses a 10-layer soil model beneath the lake, a multi-layer ice
300 formation model and up to 5-layer snow-on-ice model (Gu et al, 2015). Again, testing of
301 the CLM lake model by the authors within WRF showed computational efficiency of the
302 model with no change of even 0.1% in run time with the HRRR and RAP applications.
303 Multiple layers in lake models better represent vertical mixing processes in the lake. By
304 intention, the CLM lake model was only applied for HRRR and RAP model to smaller
305 lakes, since NOAA began at the same time to provide temperature and ice cover
306 through GLOFS for the Laurentian Great Lakes through the 3-d hydrodynamic-ice
307 model (Fujisaki-Manome et al, 2020, Anderson et al, 2018).

308 309 3.2 Lake area mask

310
311 Grid points were assigned as lake points when the fraction of lake coverage in the grid
312 cell (derived from yet finer 15" MODIS data) exceeds 50% and when HRRR gridpoint
313 elevation > 5 m above sea level (ASL, to distinguish from ocean) and is disconnected
314 from ocean areas with the 3-km land-water mask. The lake water mask is therefore
315 binary, set to either 1 or 0. This binary approach at 3 km seemed capable of capturing
316 the effect of lakes on regional heat and moisture fluxes. The alternative subgrid lake
317 fraction approach was used by ECMWF with their 9-km model (Choulga et al, 2019).

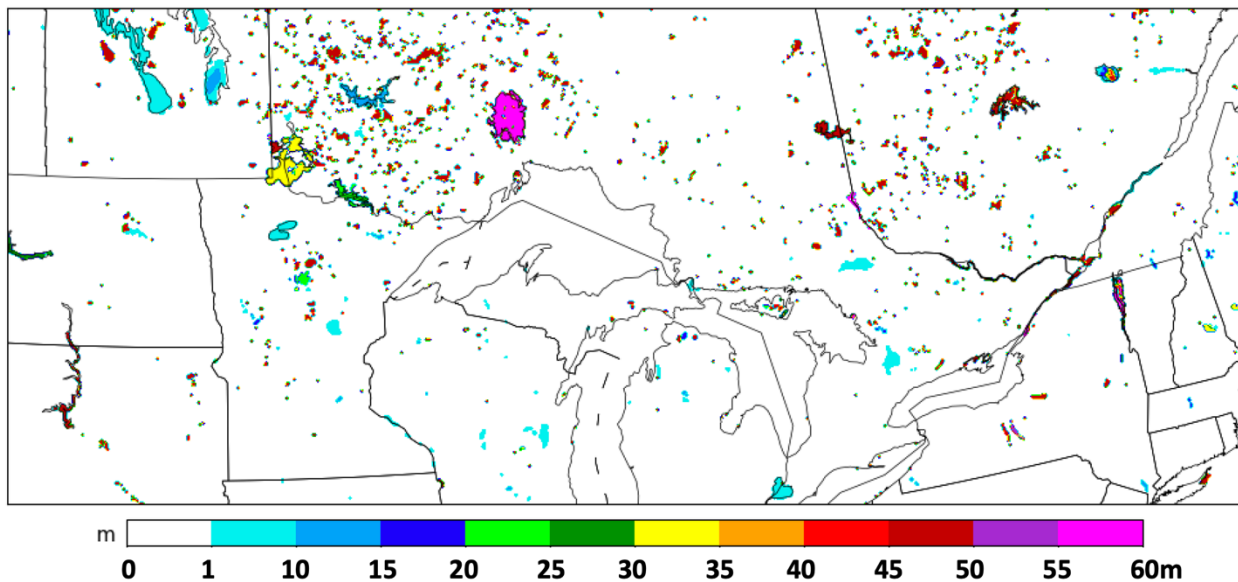
318
319 An overview of the lake number, areal coverage, and integrated volume for the 3-km
320 HRRRv4 model are depicted in Table 2. The HRRR CONUS domain (Fig. 1) is able to
321 represent 1864 separate lakes occupying 0.6% of the entire domain. These water
322 bodies represented in HRRR as "lakes" include reservoirs and larger rivers, and about
323 half of the 1864 lakes are single-gridpoint lakes. The sixteen largest lakes in the HRRR
324 CONUS domain have surface area greater than 1,000 km², nine in Canada and two on

325 the US-Canada border (Lake of the Woods and Lake St. Clair). In contrast, the five
326 Laurentian Great Lakes (Table 3) range in size from 82,000 km² (Superior) to 19,000
327 km² (Ontario), and therefore, their representation in the coupled HRRR system (Table 1)
328 is handled with 3-d hydrodynamic-ice models (Fujisaki-Manome et al, 2020).
329

330 The lake area mask for the 3-km HRRRv4 used an algorithm for identifying an ocean
331 area mask for all areas with contiguous water areas and leaving other areas also below
332 5 m ASL as near-ocean lagoon regions treated as lakes with the CLM 1-d lake model.
333 These lagoon areas separated from ocean by barrier islands in the HRRR
334 representation (Fig. 1) include the Intracoastal Waterway in Texas largely separated
335 from the Gulf of Mexico by Padre Island, Indian River in Florida largely separated from
336 the Atlantic Ocean by Merritt Island, and Lake Pontchartrain in Louisiana. This ocean-
337 contiguity technique is similar to the flood-filling technique used by ECMWF (Choulga et
338 al, 2019).
339

340 3.3. Lake depths

341
342 Lake depths for the HRRRv4-WRF-CLM lake configuration (Fig. 4) are assigned from a
343 global dataset provided by Kourzeneva et al (2012b, hereafter K12). For some smaller
344 lakes identified using the 15" MODIS land-water mask not found in K12, a 50 m depth
345 was assumed (too deep, will be reduced in future). K12 identified uncertainties in their
346 own database including estimates of lake depth and errors in coastlines. More recently,
347 ECMWF applied a 10 m depth as a default depth for these small lakes (Choulga et al,
348 2019). For many lakes in the K12 database, a single value for maximum lake depth had
349 been applied to all lake points, which results in excessive lake water volume and too
350 cold temperatures as discussed in section 5. However, the K12 database still allows
351 overall differentiation between shallow and deep lakes.
352



353
354 *Figure 4. Lake depth for small lakes in a subset of the HRRR domain.*

355

356 3.4 Turbidity

357

358 A single value for turbidity to describe absorption of downward short-wave radiation is
359 used in CLM, allowing for a moderate amount of suspended sedimentation. Subin et al
360 (2012) describe other options for variations in radiative transfer in lake bodies to capture
361 degrees of eutrophication, but these are not used here.

362

363 3.5 Salinity

364

365 The CLM lake model is configured for fresh water. The authors manually modified the
366 freezing temperature to account for non-zero salinity (Railsback, 2006) from 0°C to -5°C
367 for Mono Lake in California and Great Salt Lake (GSL) in Utah to capture the effect of
368 salinity. Other areas of water impoundment from coastal lagoons in the 3-km HRRR
369 lake representation (Fig. 1) also have, in reality, non-zero salinity (e.g., along coasts of
370 Gulf of Mexico and Atlantic Ocean) but this is not applied in HRRR/RAP. Moreover, no
371 change in freezing temperature is necessary for these areas anyway.

372

373 3.6 Elevation

374

375 The elevation value (above sea level) assigned to each lake grid point is the same
376 assigned to that from the atmospheric model, which may be different from reality, but at
377 least consistent with the atmospheric conditions. As mentioned earlier, the minimum
378 elevation above sea level of a grid point to be assigned as a lake is 5 m; other water
379 grid points are assumed to be ocean.

380

381 3.7 Special situations for CLM lake model application

382

383 The algorithm for the turbulent heat flux calculation in the CLM-lake model was mainly
384 based on Zenget al. (1998), except that roughness length scales for temperature and
385 humidity are the same as roughness length scale for momentum for its WRF-lake
386 application, while they are updated dynamically in CLM 4.5. Charusombat et al (2018)
387 showed that the same roughness length scales for temperature and salinity as that for
388 momentum could result in overestimated surface sensible and latent heat fluxes in
389 autumn and winter. Therefore, a revision to the CLMv4.5 lake model was introduced for
390 modified roughness lengths over water using modified formulations of the Coupled
391 Ocean-Atmosphere Response Experiment (COARE) algorithm as described by
392 Charusombat et al (2018) to improve surface sensible and latent heat fluxes.

393

394 For GSL with a very high value of salinity (270 ppt north of ~41.22°N with freezing point
395 of 249 K and 150 ppt south of ~41.22°N with freezing point at 263 K), a change of
396 freezing temperature to -5°C appeared to be not sufficient to keep the lake ice-free
397 during the cold outbreaks in winter in this high-elevation area. GSL is unusual in various
398 aspects – it is hypersaline (far more saline than the ocean), the largest terminal lake

399 (without outflow) in the Western Hemisphere (Belovsky et al, 2011), shallow (mean
400 depth of 5 m) and subject to very strong eutrophication (Belovsky et al, 2011).
401 According to GSL climatology the lake stays ice-free all winter, and its temperature goes
402 slightly below freezing only for a very short period in January and February. Thus, we
403 presume that the CLM lake model needs to allow turbidity variation (see section 3.4). A
404 solution to this representation problem was use of a bi-weekly climatology over each 1-
405 year period to bound the cycled GSL temperature at initial forecast time not to deviate
406 more than +/- 3°C from the climatological value interpolated to the current day of year.
407 Also, using special code, GSL was forced stay ice-free for the whole year as observed.
408

409 3.8 Time step

410
411 The CLM lake model within the HRRR/RAP weather models was run with the same time
412 step as for other physical processes in the HRRR model (20 s) and the RAP model (60
413 s). Again, even with this relatively high frequency for calling the CLM lake model, the
414 computational expense was extremely small, less than 0.1% of overall HRRR run time.
415

416 **4 Initialization for small lake temps by cycling with ongoing atmospheric** 417 **predictions – a strategy**

418
419
420 The central strategy described in this paper is to use accurate, ongoing atmospheric
421 forcing with a computationally inexpensive 1-d lake model to obtain an equilibrium state
422 of a lake temperature profile. This technique responds appropriately to strong changes
423 in atmospheric forcing (e.g., cold air outbreak or excessive heat events). With the
424 NOAA HRRR and RAP atmospheric models performing hourly data assimilation of a
425 broad set of hourly observations, accurate atmospheric forcing is available.
426

427 The RAP and HRRR hourly data assimilation cycles include these aspects, all of which
428 are important for cycling initialization of inland lakes. First, cloud assimilation (from
429 satellite and ceilometer data) to ensure accurate shortwave and longwave radiation
430 fields (Benjamin et al 2021). Second, radar reflectivity data are assimilated as part of a
431 3-km ensemble data assimilation system to ensure accurate short-range precipitation
432 (Weygandt et al, 2022, D22, J22, Benjamin et al, 2016). Finally, 2 m air temperature
433 and moisture and 10 m wind observations are effectively assimilated (i.e., producing
434 more accurate predictions) including representation through the boundary layer using
435 pseudo-innovations (James and Benjamin, 2017, meaning estimated observation-
436 background forecast differences but not actual). Other information on the HRRR/RAP
437 data assimilation is provided by Benjamin et al (2016) and D22.
438

439 The cycling of the 10-level CLM lake model within the then-experimental HRRRv4
440 started on 24 August 2018. After 10 days of cycling (Fig. 4), differences in lake
441 temperatures between HRRRv4 and the operational HRRRv3 using interpolated NSST

442 data were evident of 5-15°F (3-12°C or 276-285 K), showing that the adjustment with
 443 realistic atmospheric conditions and use of the CLM lake model with roughly accurate
 444 lake depth data was very effective.
 445

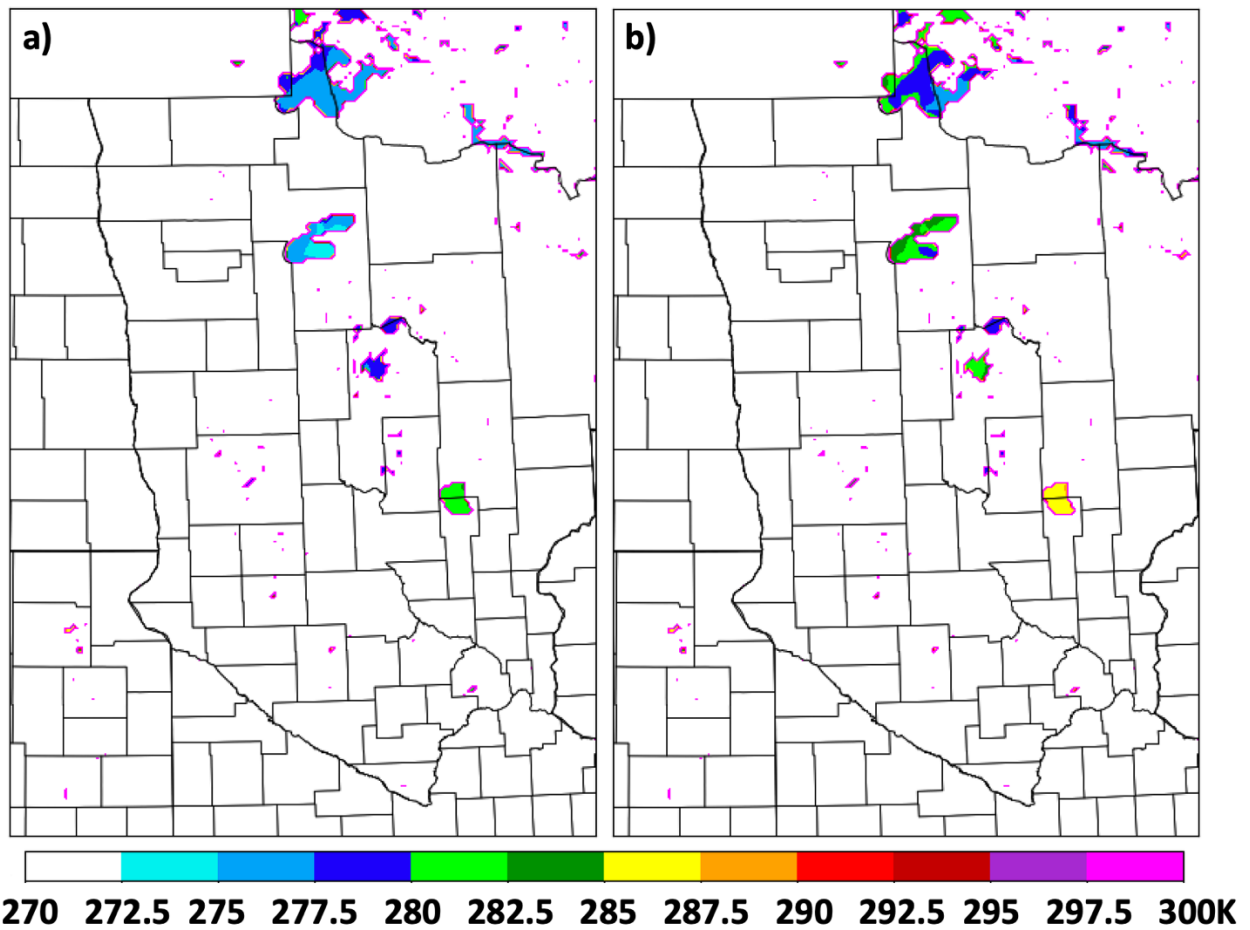
Consequences (to right) from strategy for lake initialization (below)	Coupling lake and atmosphere within initialization	Lake temps in spring-summer	Lake temps in fall
SST interpolation to small lakes	None	Much too cold, especially for shallow lakes	Still generally too cold but intermittently too warm after cold-air outbreaks.
Lake annual variation forced by reanalysis atmospheric data – 1-way cycling from atmospheric forcing	1-way	More accurate. No weather regime variation in a given year	More accurate. Will not capture variation from weather regimes in a given year.
Daily updating with satellite data	None	More accurate but cannot keep up with changes during cloudy periods.	More accurate but cannot keep up with changes during cloudy periods.
2-way coupled cycling	2-way	More accurate including response to specific yearly/seasonal anomalies.	More accurate including yearly/seasonal anomalies

446
 447 *Table 4. Expected seasonal lake-atmosphere temperature consequences from different*
 448 *lake initialization strategies*
 449

450 Possible approaches for initializing lake temperatures are summarized in Table 4. The
 451 simplest option is via larger-scale water temperature data (SST data) with horizontal
 452 interpolation to smaller water areas including inland lakes and reservoirs; this was the
 453 previous strategy for the HRRRv3 and older RAP models before introduction of cycling
 454 using the CLM lake model. An alternate strategy is to run lake models over a multi-year
 455 period forced by reanalysis atmospheric data (ERA-Interim) as described by Balsamo et
 456 al (2012), Dutra et al (2010), and Balsamo (2013) for the ECMWF to obtain a yearly
 457 varying climatology of lake temperature for all lakes represented. This method will
 458 capture the mean annual variation of lake temperatures. However, due to multi-year
 459 averaging, it cannot represent anomalous conditions in a given year (sustained heat or
 460 sustained cold conditions), which can modify temperatures especially for shallow lakes
 461 by several K within 1-2 weeks. Use of daily updating from satellite data can be effective
 462 (e.g., MetOffice – Fiedler et al, 2014) under clear-sky conditions. Full cycling of the lake
 463 model within an ongoing coupled weather model, the strategy described in this paper,
 464 can represent the lingering effects of anomalously warm or cold weather upon lake
 465 temperatures and the resultant fluxes.

466
467
468
469
470
471
472
473
474
475
476
477
478
479

The 2-way coupled cycling (Table 4) used now in the HRRR and RAP models benefit via hourly data assimilation using latest hourly observations both for the atmosphere (D22) and land-surface snow conditions (Benjamin et al 2021). In the 3-km HRRR model, the 3-d state of the atmosphere, land surface, and inland lake conditions are advanced on 20-second time steps using the HRRR-specific configuration (described in D22) of the WRF model (Powers et al, 2017; Mallard et al, 2015). As atmospheric conditions change every 20 s (including temperature, moisture, wind, and radiation), the exchange of heat, moisture, and momentum between inland lake points and the atmosphere also vary. Lake temperature is not modified in the hourly data assimilation step, but the ongoing exchange recalculated every 20 s forces an evolution of lake conditions to values consistent with atmospheric conditions. ECMWF applies a similar ongoing cycling for lake prognostic variables (ECMWF, 2020) for lake initialization.



480
481
482
483
484
485

Figure 5. Lake surface temperatures from 18-h forecasts valid at 1500 UTC 3 September 2018 for a) operational HRRRv3 using NSST for lake temperatures, and b) then-experimental HRRRv4 with CLM lake model and cycling.

486 A similar challenge is initialization of lake ice cover. Similar to the treatment for lake
487 temperature, cycling of a multi-level lake model (like the CLM lake model) can provide
488 an alternative, adaptive-in-time method for lake-ice initialization. NOAA has used in the
489 HRRR and RAP the daily IMS ice cover product¹ (US National Ice Center, 2008) for
490 binary (non-fractional) lake ice cover. The IMS ice cover is used for oceans and large
491 lakes (e.g., for RAP for Great Slave Lake and Great Bear Lake in northern Canada). For
492 small lakes below the resolution of the IMS ice map, lakes stayed open for the winter.
493 Starting with HRRRv4 and RAPv5, ice concentration from the NOAA global model is
494 used for oceans, FVCOM ice fraction is used for the Great Lakes, and ice fraction from
495 the CLM lake model for small lakes.

496

497 **5 Results**

498

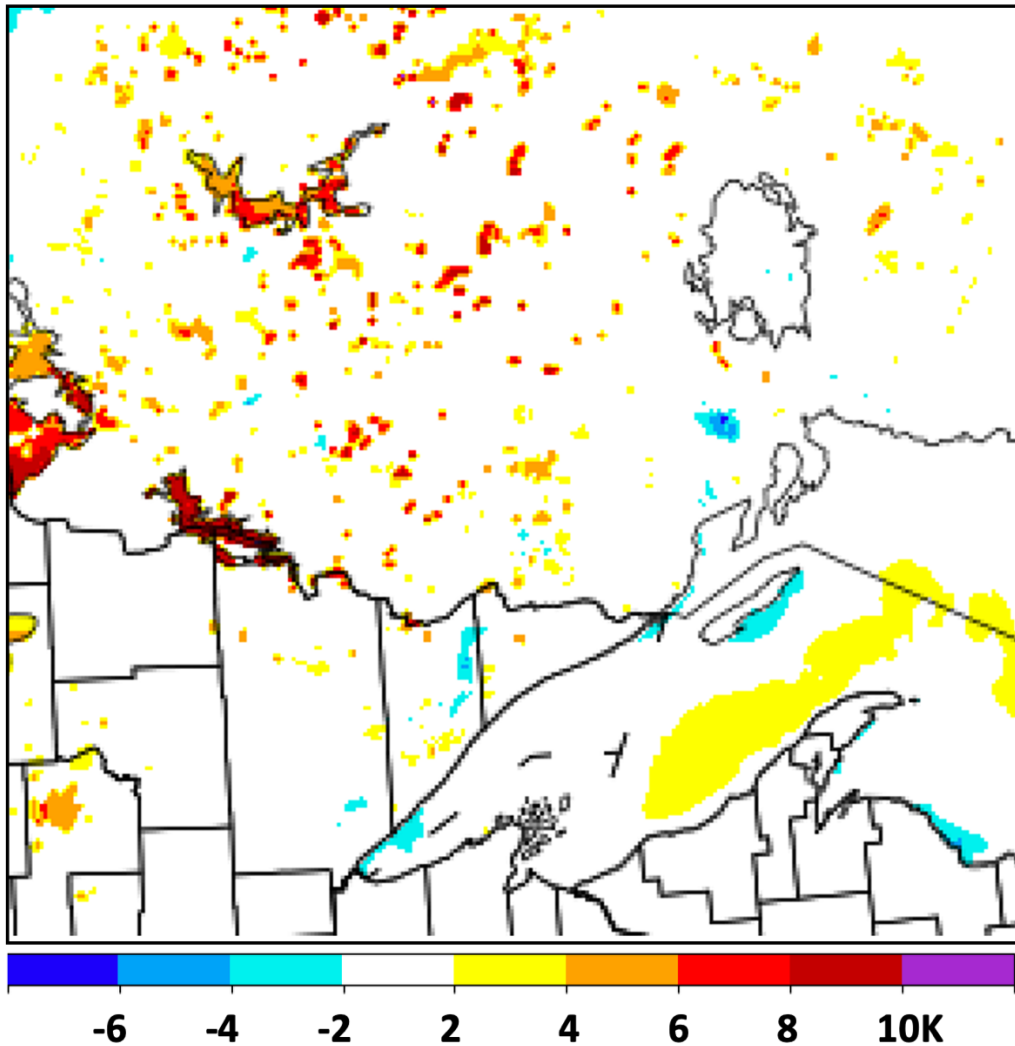
499 In this section, we describe comparisons of lake surface temperature evolution between
500 the CLM implementation described here and the lake specification through interpolation
501 from the NSST dataset (Fig. 2) at lakes in the United States and southern Canada.

502

503 Comparisons during 2018–2019 were drawn from real-time simulations from the then-
504 operational HRRRv3 (using interpolated SST) and the then-experimental HRRRv4
505 (using CLM). More recent comparisons were made for March–November 2021 between
506 the operational HRRRv4 (using CLM) and interpolated NSST values (as used in 2019-
507 2020 for HRRRv3). In addition, the CLM and NSST values were compared to in situ
508 observations where available and also to satellite-based estimates defined below.

509

¹ <https://usicecenter.gov/Products/ImsHome>



510
511

512 *Figure 6. Difference (K) in lake surface temperatures between versions of HRRR*
 513 *model using cycled lake-model values (HRRRv4) and using interpolated NSST data*
 514 *(HRRRv3). Valid 1300 UTC 13 October 2019, and also includes differences from use*
 515 *of FVCOM lake model in HRRRv4 (Fujisaki-Manome et al, 2020).*

516

517 5.1 Cases from 2018 – 2019

518

519 Introduction of the CLM lake model forced by ongoing HRRRv4 atmospheric conditions
 520 (i.e., cycling) allowed, within only 10 days, an increase in lake temperatures for Red
 521 Lake and Lake of the Woods (both in Minnesota) from 3 K to over 10 K (Fig. 5) in
 522 September 2018. A comparison in skin temperature for a year later (October 2019)
 523 between versions of the HRRR model (HRRRv4 with lake cycling vs. HRRRv3)
 524 including differences from with and without lake cycling is shown in Fig. 6. Higher
 525 temperatures were evident for the Minnesota/Ontario lakes from cycling (vs. NSST
 526 interpolation). HRRRv4 also included coupling with the 3-d FVCOM lake model for

527 the Laurentian Great Lakes, showing areas of upwelling with associated cooler water
 528 over Lake Superior in Fig. 6 from predominant westerly to southwesterly near-surface
 529 wind at this time.

530
 531

Lake number	Lake name	State/province, country	HRRR l point	HRRR j point	Area (km ²)	Depth used (m)	Ice free?
1	Simcoe	ON, CA	1378	799		6	N
2	St. Clair	ON/MI, CA/US	1302	709	1240	6	N
3	Champlain	VT/NY, US	1534	835		77	N
4	Sebago	ME, US	1610	833		33	N
5	Okefenokee	FL, US	1459	145	1510	3	Yes
6	Pontchartrain	LA, US	1136	224	2180	10	Yes
7	Intracoastal Waterway (near Corpus Christi, TX)	TX, US	905	128	3300	10	Yes
8	Salton Sea	CA, US	337	387		9	Yes
9	Tahoe	NV/CA, US	259	628		313	N
10	Great Salt	UT, US	486	653	3050	3	Yes
11	Utah	UT, US	496	622		3	N
12	Bear	ID/UT, US	518	684		29	N
13	Sakakawea	ND, US	790	868		27	N
14	Winnebago	WI, US	1143	742		7	N
15	Lower Red	MN, US	961	880		5	N
16	Lake of the Woods	MB/MN, CA/US	965	919	3030	32	N
17	Manitoba	MB, CA	879	972	3240	5	N
18	Winnipeg	MB, CA	916	977	13270	8	N
19	Nipigon	ON, CA	956	956	5410	55	N

532 *Table 5. Lakes for comparison of lake surface temperatures between HRRRv4/CLM,*
 533 *NASA SPOrT, NSST, and in situ observations as shown in Figs. 7 and 8. Area is*
 534 *shown for lakes >1000 km². Lake depths are constant within each lake except for lakes*
 535 *2, 3, and 18. See Fig. 4 for example map of lake depth used in HRRR. Specific HRRR*
 536 *i/j 3-km grid points (indicated in table) were selected from HRRR data for each lake.*

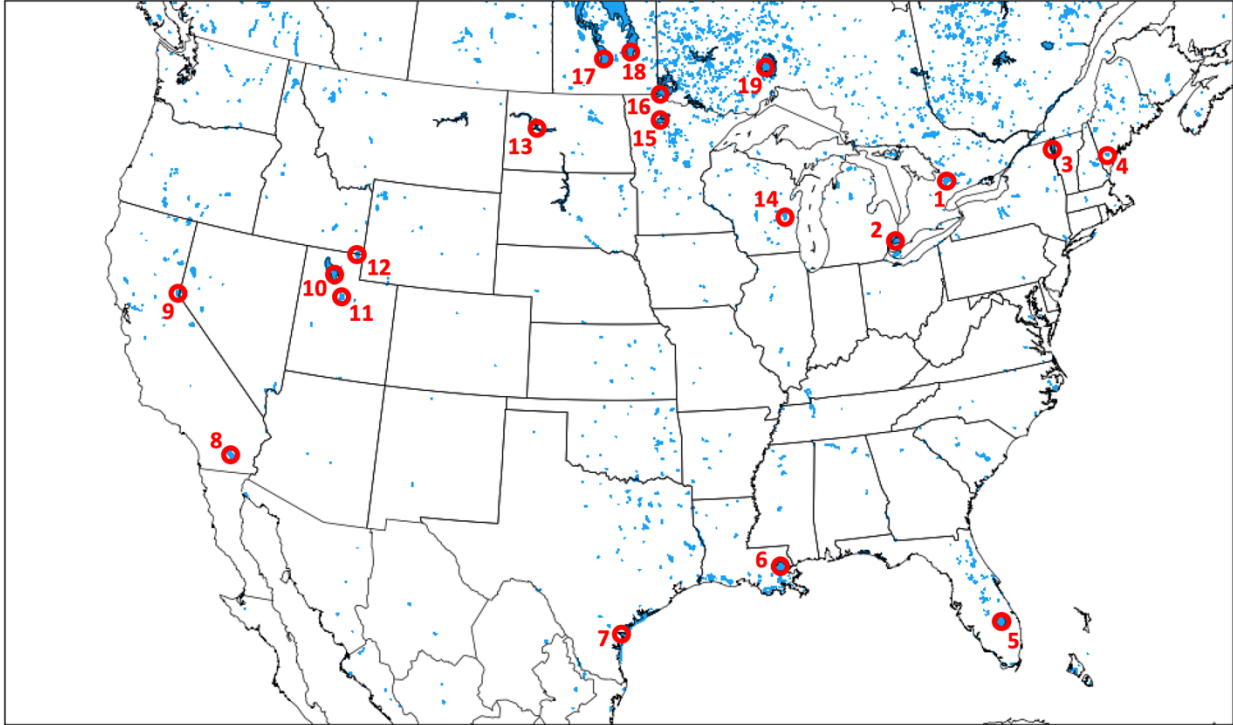
537

538
539

Name of Lake	No. from Tab. 5	Source of Observation	Depth of Sensor (m)	URL
Lake St. Clair	2	ECCC	6	https://www.ndbc.noaa.gov/station_page.php?station=45147
Lake Champlain - Schuyler Reef	3	GLERL	0.45	https://www.ndbc.noaa.gov/station_page.php?station=45195
Sebago Lake @ Lower	4	Portland Water District Buoy	Est 1	https://www.pwd.org/sebago-lake-monitoring-buoy
Lake Pontchartrain @ New Canal Station	6	NOAA/ National Ocean Service	0.6	https://www.ndbc.noaa.gov/station_page.php?station=nwcl1
Intracoastal Waterway @ Baffin Bay near Padre Island	7	Texas Coastal Ocean Observing Network	unknown	https://www.ndbc.noaa.gov/station_page.php?station=babt2
Lake Tahoe	9	NASA/JPL	0.5	https://laketahoe.jpl.nasa.gov/get_imp_weather
Utah Lake @ Provo Marina	11	Utah DWQ Water Quality Network	unknown	https://wqdatalive.com/public/669
Bear Lake	12	Utah DNR State Parks	unknown	https://stateparks.utah.gov/parks/bear-lake/current-conditions/
Lake Sakakawea @ Missouri River near Williston, ND	13	USGS	unknown	https://waterdata.usgs.gov/monitoring-location/06330000/#parameterCode=00065&period=P7D

540
541
542

Table 6. Sources of available in situ data among 19 lakes in Table 5.



543
544

545 *Figure 7. Locations of 19 lakes (see Table 5) used for the lake surface temperature*
546 *intercomparison in this paper in Fig. 8. These lakes are shown as mapped onto the 3-*
547 *km CONUS HRRR model domain.*

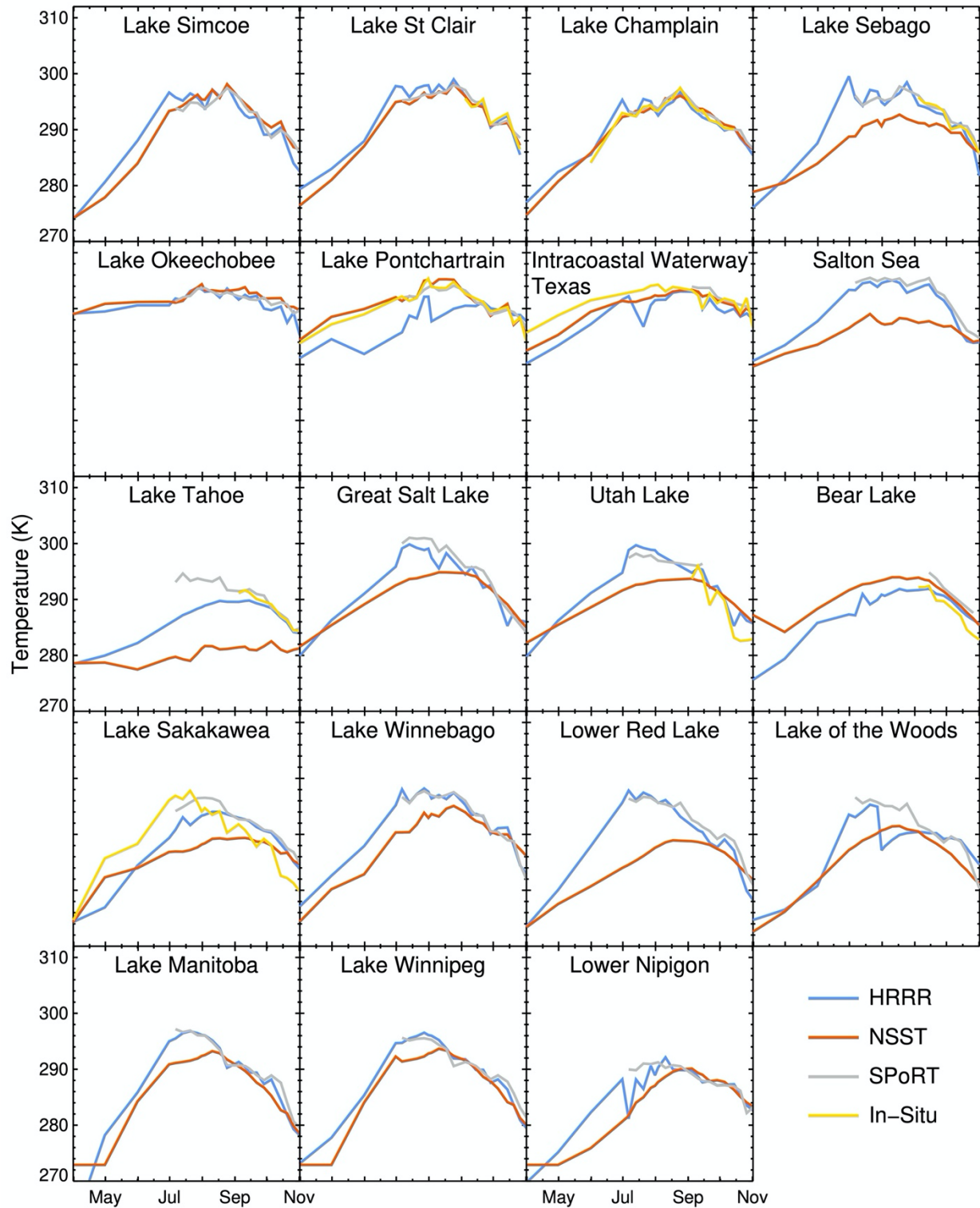
548
549

550 5.2 Comparisons of different lake temperature estimates for 19 lakes from lower 48
551 US and southern Canada during 2021.

552

553 During a period from March to November 2021, a comparison was made of lake
554 surface temperatures between the cycled HRRRv4-CLM values and those from three
555 other estimates from NASA, NOAA, and in situ observations. A geographically diverse
556 set of 19 lakes over the lower 48 United States and southern Canada was selected for
557 these comparisons as listed in Table 5 and shown in Fig. 7. Lakes selected included
558 near-ocean lagoon areas separated from ocean areas by coastal land as resolved by
559 the 3-km land-water mask as discussed in section 3.2. The water areas also included a
560 reservoir (Lake Sakakawea). Some of these lakes are dimictic or polymictic (with ice
561 cover part of each year, Lewis 1983) but five of them do not experience any ice cover
562 (Table 5), and lakes 5, 6, 7, and 8 are monomictic. The CLM lake model was cycled for
563 all these lakes in the 3-km HRRRv4 model. The 19 lakes included seven lakes with a
564 surface area greater than 1,000 km². The March-November evaluation period include
565 the spring-summer warming period and the cooling period in autumn. Data points were
566 obtained monthly for March-August and weekly for September-November.

567
568



569
 570
 571
 572
 573

Figure 8. Lake surface temperatures in 2021 (April-October) from the 19 selected lakes (Table 5, Fig. 7) from HRRR-CLM-cycled, NSST, SPoRT, and in situ data.

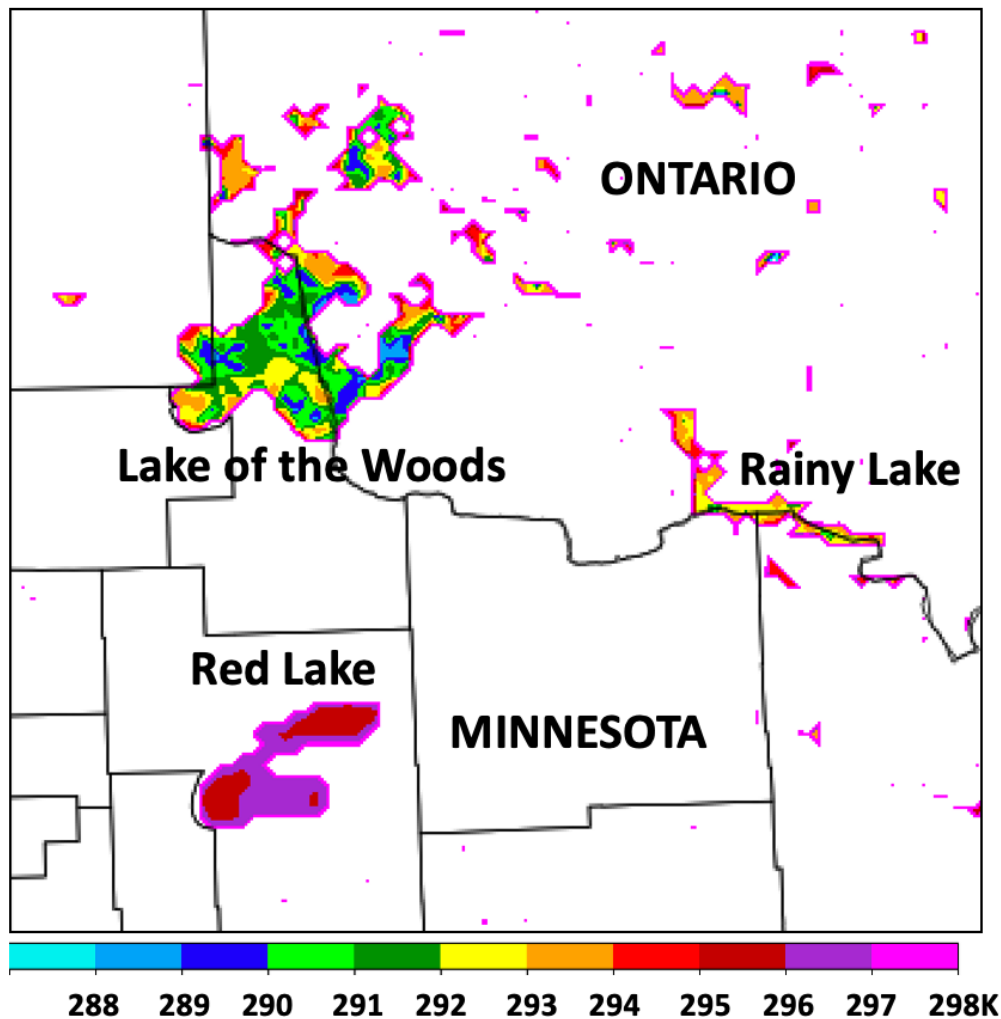
574
575 The HRRRv4-CLM values for these 19 lakes were compared with first, an estimate from
576 NASA SPoRT (Short-Term Prediction Research and Transition) real-time surface water
577 temperature composite including time-weighted MODIS and VIIRS data for inland lakes
578 (NASA, 2021, Kelley et al, 2021). The SPoRT estimates are similar to the satellite-
579 based lake temperature estimates from the Met Office (Fiedler et al 2014). The SPoRT
580 composite is valid from the surface to 2 m depth and is averaged over a 7-day period to
581 mitigate for cloud cover on a given day. A second lake temperature estimate is that from
582 NSST, as discussed earlier. Third, in situ surface water temperature observations were
583 available from observing platforms in nine of the 19 lakes (Table 6). The platforms are
584 operated by Federal, state, and local government agencies and a regional ocean
585 observing system. The depths of the water temperature observations were only
586 available at four of the nine platforms. At these four sites, the depth ranged from 0.45 to
587 0.9 m.

588
589 In general, the HRRRv4-CLM-cycled lake surface temperatures showed the anticipated
590 difference from NSST values with quicker summer warming from HRRR-CLM cycling for
591 all lakes except the southern 3 lakes (5, 6, 7 in Table 5, with Lakes 6 and 7 essentially
592 lagoons in close proximity to the ocean) and Bear Lake in UT/ID (Lake 12, 39 m depth).
593 The NSST estimates were colder for spring through summer than HRRR values for 15
594 of the 19 lakes, a consequence from the NSST estimate via horizontal interpolation from
595 deeper bodies of water.

596
597 For the nine lakes with in situ observations (Table 6), the HRRR-CLM-cycled lake
598 temperatures are generally able to better capture weekly variability in summer and
599 autumn months, associated with windy periods increasing mixing or relatively warm and
600 cool weather periods or varying amounts of cloud cover. This can be seen, for
601 example, at Utah Lake and the Intracoastal Waterway west of Padre Island in Texas
602 (note cooling from passage of Hurricane Nicholas in mid-September). The most
603 dramatic improvement of HRRR-CLM over NSST lake temperatures is seen at Lake
604 Tahoe and lakes 14-19 in the northern region, with NSST estimates 5-10 K too cool. At
605 two of the lakes with in situ observations, the Intracoastal Waterway (linked to the
606 ocean) and Lake Pontchartrain, both lagoons linked to the ocean, NSST estimates are
607 generally closer than HRRR-CLM to the observations.

608
609 HRRR-CLM lake surface temperatures matched in situ observations well for the
610 northern lakes, usually within 1-2 K. In contrast, the lake temperature values from
611 SPoRT were generally warmer than HRRR or in situ observations in the autumn period.
612 The SPoRT observations showed a strong confirmation of HRRR-CLM-cycled lake
613 temperatures for lakes in the western US (Lakes 8-13) and most lakes in the northern
614 areas (Lakes 4, 14-19). Finally, the HRRR-CLM-cycled lake temperatures during this
615 period often varied strongly from the NSST estimates, with differences of up to 5-10 K
616 (largest difference with Red Lake, Lake 15). The effect of lake depth was evident with
617 a faster transition to fully mixed lakes for shallow lakes (e.g., 5 m depth for Red Lake in

618 MN, Lake 15 in Table 5) but subject to more temporal and horizontal variation for
 619 deeper lakes. Fig. 9 showed a strong intralake variation of 7 K across Lake of the
 620 Woods (32 m depth) in the HRRR-CLM estimate in contrast with very little variation (< 1
 621 K) across Red Lake. Due to a lack of high-resolution observations of lake surface
 622 temperatures, it is difficult to determine which intralake variations are more realistic.
 623 However, we think some of these intralake contrasts from HRRR-CLM may be
 624 exaggerated from actual values, possibly requiring a future introduction of a small
 625 temperature exchange rate (diffusion) between adjacent lake columns. Differences in
 626 skin temperature (e.g., SPoRT) and bulk temperature (e.g., in situ) for lakes have been
 627 noted (e.g., Wilson et al, 2013) of up to 0.5 K, but the HRRR vs. NSST differences in
 628 this study are generally much larger than this magnitude.
 629



630 *Fig. 9. HRRRv4-CLM lake surface temperature (K) for 1500 UTC 31 July 2021 for area*
 631 *over northern Minnesota (US) and southwestern Ontario (Canada).*
 632

633
 634 The main deficiencies evident so far with the HRRR-CLM lake temperatures appear to
 635 be associated with errors in lake depth values. On the average, the current specified

636 values for mean lake depth for most lakes are too deep compared to reality, since the
637 preprocessing with the K12 dataset simply assigned a single lake depth value
638 (maximum or mean) to all grid points for that lake even up to the modeled lake points
639 adjacent to land, as shown in Table 5 for 16 or the 19 lakes studied. We also noted too-
640 low lake temperatures in HRRRv4 for lake grid points at the western edge of a few lakes
641 (e.g., Tahoe, Sebago (ME), Cayuga (NY), Champlain), all relatively deep lakes (Fig. 5,
642 Table 5). We attribute this to 1-d upwelling from insufficient bathymetry data resulting in
643 cylinder-like lake volumes with constant lake depths, therefore with a) too-deep lake-
644 edge pixels coinciding with b) strong winds coming off from land areas with
645 predominantly westerly winds. This deficient effect was not widespread for the HRRR
646 model and did not affect the overall results. Again, this behavior is attributed to the
647 behavior of the lake model over integrations with the inaccurate lake depth information
648 and not to the lake cycling initialization design.

649

650

651 **6 Conclusions**

652

653 We report here on the first use of a small-lake model (CLM4.5, 10 layer) in US NOAA
654 NWP models along with an ongoing cycling of lake temperatures since 2018 to initialize
655 lake temperatures in each prediction. These models are the 3-km HRRRv4 (D22, J22)
656 and 13-km RAPv5 hourly updated models, both of which became operational in
657 December 2020 after cycling since August 2018. At 3-km grid spacing, the HRRR
658 model applied this small-lake modeling and assimilation to 1864 small lakes varying in
659 size from about 10 km² (single grid point) to 14 larger lakes over 1000 km² in surface
660 area, but not including the Laurentian Great Lakes. The effectiveness of introducing the
661 multi-layer lake model into the HRRR and RAP models was completely dependent on
662 the initialization for lake temperatures. The introduction of a cycling capability through
663 the hourly assimilation allowed the lake temperatures to evolve to accurate values,
664 consistent with recent weather. In this paper, we describe the lake cycling applied for
665 the NOAA regional 3-km HRRR and 13-km RAP weather models including the coupled
666 1-d CLM lake model. We also show some comparisons with other estimates of lake
667 surface temperatures. From those comparisons, the cycled lake surface temperatures
668 from the 3-km HRRR model were found to be reasonably accurate. HRRR lake surface
669 temperatures were found to be generally within 1 K of in situ observations and within 2
670 K of the SPoRT estimates. Finally, NSST estimates of small-lake temperatures were
671 found to often differ from in situ observations and HRRR estimates by 5-12 K. Other
672 differences between lake-cycled HRRR estimates and SST-based estimates were up to
673 10-15 K.

674

675 From these initial results, we conclude that the lake-cycling initialization for small lakes
676 has been effective overall, owing to accurate hourly estimates of near-surface
677 temperature, moisture and winds, and shortwave and longwave estimates provided to
678 the 1-d CLM lake model every time step (20 s for 3-km HRRR model). The HRRR-CLM
679 treatment also allows some inland lakes to freeze in winter, which is more consistent

680 with observations. The lake cycling strategy is similar to that initialization method used
681 by ECMWF for its 9-km (as of 2021) IFS (Integrated Forecast System) and using a
682 binary lake mask in the 3-km HRRR model.

683
684 One deficiency noted was development of too-cold lake surface for a few lakes on their
685 western boundary. We attribute this to the incorrect bathymetry data with constant lake
686 depth (e.g., see caption for Table 5) causing an excessive 1-d upwelling from too-deep
687 lake depth at western shores for these lakes. This issue is being addressed with a
688 current project to improve lake bathymetry data for which results will be reported in the
689 future. Also, HRRR-CLM cycling gave poorer results than NSST at least for Lake
690 Pontchartrain (Lake #6 in Table 5), suggesting to use NSST for near-ocean lagoon
691 areas. More investigation is needed for strong intralake variations overall in HRRR-
692 CLM-cycling representation (e.g., Lake of the Woods in Fig. 9) and possible introduction
693 of horizontal diffusion of temperature between adjacent lake points.

694
695 US NWS forecasters have reported much improved near-surface temperature and
696 dewpoint predictions in the vicinity of small lakes from the 3-km HRRR model in 2021
697 since the implementation of the 1-d CLM lake model and lake-cycling initialization.
698 Again, this effort complements the coupling of the HRRR model with the 3-d FVCOM
699 hydrodynamical lake model for the Laurentian Great Lakes (Fujisaki-Manome et al,
700 2020) design to improve lake-effect snow predictions. These efforts are the most
701 advanced lake-coupling and lake-initialization efforts at this point in US NOAA weather
702 models.

703
704 Overall, the improved lake temperatures from the lake cycling initialization technique
705 driven over a 3-year period by accurate atmospheric conditions described here results
706 in improved fluxes of heat and moisture over using SST interpolation and improved
707 nearby predictions of atmospheric 2 m temperature and 2 m moisture.

708 **Code availability**

709 This research used WRF version 3.9.1 including use of the option with the CLM lake
710 model. All code is available from the National Center for Atmospheric Research
711 (NCAR) at https://www2.mmm.ucar.edu/wrf/users/download/get_sources.html

712 **Data availability**

713 HRRR data (including lake surface temperature data under ‘skin temperature’ field) are
714 publicly available via archives hosted by Amazon Web Services
715 (<https://registry.opendata.aws/noaa-hrrr-pds/>) and Google Cloud Platform
716 ([https://console.cloud.google.com/marketplace/product/noaa-public/hrrr?project=python-
717 232920&pli=1](https://console.cloud.google.com/marketplace/product/noaa-public/hrrr?project=python-232920&pli=1)).

718 **Author contributions**

719 SB, TS, and EJ planned the design. TS and EJ carried out the actual coding for
720 modeling, data assimilation and scripts. EJ, SB, JK, and SK extracted data from
721 experiments and other sources. EJ and JK analyzed the results. SB wrote the

722 manuscript draft and led its revision. EA, AFM, JK, GM, AG and PC (along with TS and
723 EJ) reviewed and edited the manuscript.

724 **Acknowledgments**

725 Credit is due to the WRF model team at NCAR (Jimmy Dudhia) for their help in applying
726 the CLM lake model for the HRRR and RAP applications of the WRF model. We
727 greatly appreciate our NOAA colleague, Thomas Hamill (NOAA PSL), for Fig. 3 from
728 another already published article by him. We also thank Frank J. LaFontaine and Kevin
729 K. Fuell of the NASA SPoRT Team for providing archived Northern Hemisphere SST
730 composites. Thanks also to Rob Cifelli of NOAA/PSL for a very helpful review of our
731 manuscript. This work was supported by NOAA Research base funding.

732 **References**

733 Anderson, E. J., Fujisaki-Manome, A., Kessler, J., Lang, G. A., Chu, P. Y., Kelley, J. G.
734 W., et al.: Ice forecasting in the next-generation Great Lakes Operational Forecast
735 System (GLOFS). *Journal of Marine Science and Engineering*, 6(123),
736 <https://doi.org/10.3390/jmse6040123>, 2018

737 Balsamo, G., Salgado, R., Dutra, E., Boussetta, S., Stockdale, T., Potes, M.: On the
738 contribution of lakes in predicting near-surface temperature in a global weather
739 forecasting model. *Tellus A: Dynamic Meteorology and Oceanography*.
740 <https://doi.org/10.3402/tellusa.v64i0.15829>, 2012

741 Balsamo, G., Interactive lakes in the Integrated Forecast System. ECMWF Newsletter
742 137, p. 30-34. 10.21957/rffv1gir, 2013.

743
744 Balsamo, G., Mahfouf, J.-F.: Les schémas de surface continentale pour le suivi et la
745 prévision du système Terre au CEPMMT. *La Météorologie*, 108, 77-81, 2020.

746
747 Belovsky, G., Stephens, D., Perschon, C., et al.: The Great Salt Lake Ecosystem (Utah,
748 USA): long term data and a structural equation approach, *Ecosphere*, 2, 1-40,
749 doi.org/10.1890/ES10-00091.1, 2011.

750
751 Benjamin, S.G., D. Devenyi, S.S. Weygandt, K.J. Brundage, J.M. Brown, G. Grell, D.
752 Kim, B.E. Schwartz, T.G. Smirnova, T.L. Smith, G.S. Manikin: An hourly
753 assimilation/forecast cycle: the RUC. *Mon. Wea. Rev.*, 132, 495-518. 2004.

754 Benjamin, S.G., B.D. Jamison, W.R. Moninger, S. R. Sahm, B. Schwartz, T.W.
755 Schlatter: Relative short-range forecast impact from aircraft, profiler, radiosonde, VAD,
756 GPS-PW, METAR, and mesonet observations via the RUC hourly assimilation
757 cycle. *Mon. Wea. Rev.*, 138, 1319-1343. 2010.

758 Benjamin, S. G., S.S. Weygandt, M. Hu, C.A. Alexander, T.G. Smirnova, J.B. Olson,
759 J.M. Brown, E. James, D.C. Dowell, G.A. Grell, H. Lin, S.E. Peckham, T.L. Smith, W.R.
760 Moninger, G.S. Manikin: A North American hourly assimilation and model forecast

761 cycle: The Rapid Refresh. *Mon. Wea. Rev.*, 144, 1669-
762 1694. <http://dx.doi.org/10.1175/MWR-D-15-0242.1>. 2016.

763 Benjamin, S.G., E.P. James, M. Hu, C.R. Alexander, T.T. Ladwig, J.M. Brown, S.S.
764 Weygandt, D.D. Turner, P. Minnis, W.L. Smith, Jr., and A. Heidinger: Stratiform cloud-
765 hydrometeor assimilation for HRRR and RAP model short-range weather prediction.
766 *Mon. Wea. Rev.*, 149, 2673-2694. <https://doi.org/10.1175/MWR-D-20-0319.1>. 2021.

767 Benjamin, S.G., T.G. Smirnova, E.P. James, L.-F. Lin, M. Hu, D.D. Turner, and S. He:
768 Land-snow assimilation including a moderately coupled initialization method applied to
769 NWP. *J. Hydromet.*, 23, 825-845, <https://doi.org/10.1175/JHM-D-21-0198.1>. 2022.
770

771 Boussetta, S.; Balsamo, G.; Arduini, G.; Dutra, E.; McNorton, J.; Choulga, M.; Agustí-
772 Panareda, A.; Beljaars, A.; Wedi, N.; Muñoz-Sabater, J.; de Rosnay, P.; Sandu, I.;
773 Hadade, I.; Carver, G.; Mazzetti, C.; Prudhomme, C.; Yamazaki, D.; Zsoter, E.:
774 ECLand: The ECMWF Land Surface Modelling System. *Atmosphere*, 12, 723.
775 <https://doi.org/10.3390/atmos12060723>, 2021.
776

777 Charusombat, U., Fujisaki-Manome, A., Gronewold, A. D., Lofgren, B. M., Anderson, E.
778 J., Blanken, P. D., Spence, C., Lenters, J. D., Xiao, C., Fitzpatrick, L. E., and Cutrell, G.:
779 Evaluating and improving modeled turbulent heat fluxes across the North American
780 Great Lakes, *Hydrol. Earth Syst. Sci.*, 22, 5559–5578, [https://doi.org/10.5194/hess-22-](https://doi.org/10.5194/hess-22-5559-2018)
781 5559-2018, 2018.
782

783 Chen, C., Beardsley, R. C., & Cowles, G.: An unstructured grid, finite volume coastal
784 ocean model (FVCOM) system. *Oceanography*, 19(1), 78–89.
785 <https://doi.org/10.5670/oceanog.2006.92>, 2006.
786

787 Chen, C., Beardsley, R., Cowles, G., Qi, J., Lai, Z., Gao, G., et al.: An unstructured grid,
788 Finite-Volume Coastal Ocean Model FVCOM -- User Manual. *Tech. Rep.*,
789 *SMAS/UMASSD-13-0701, Sch. for Mar. Sci. and Technol., Univ. of Mass. Dartmouth,*
790 *New Bedford.*, 416 pp., 2013
791

792 Choulga, M., Kourzeneva, E., Balsamo, G., Boussetta, S., and Wedi, N.: Upgraded
793 global mapping information for earth system modelling: an application to surface water
794 depth at the ECMWF, *Hydrol. Earth Syst. Sci.*, 23, 4051–4076,
795 <https://doi.org/10.5194/hess-23-4051-2019>, 2019.
796

797 De Pondeva, M.S.F.V., Manikin, G.S., DiMego, G., Benjamin, S.G., Parrish, D.F.,
798 Purser, R.J., Wu. W.-S., Horel, J.D., Myrick, D.T., Lin, Y., Aune, R.M., Keyser, D.,
799 Colman, B., Mann, G., and Vavra, J.: The Real-Time Mesoscale Analysis at NOAA's
800 National Centers for Environmental Prediction: Current status and development. *Wea.*
801 *Forecasting*, 26, 593-612, <https://doi.org/10.1175/WAF-D-10-05037.1>, 2011
802

803 Dirmeyer, P.A., Halder, S., Bombardi, R.: On the harvest of predictability from land
804 states in a global forecast model. *J. Geophys. Res. Atmospheres*, 123, 13,111-
805 13,127. <https://doi.org/10.1029/2018JD029103>, 2018.

806

819 Dowell, D. C., C. R. Alexander, E. P. James, S. S. Weygandt, S. G. Benjamin, G. S.
820 Manikin, B. T. Blake, J. M. Brown, J. B. Olson, M. Hu, T. G. Smirnova, T. Ladwig, J. S.
821 Kenyon, R. Ahmadov, D. D. Turner, J. D. Duda, and T. I. Alcott: The High-Resolution
822 Rapid Refresh (HRRR): An hourly updating convection-allowing forecast model. Part I:
823 Motivation and system description. *Wea. Forecasting*, 150,
824 <https://doi.org/10.1175/WAF-D-21-0151.1>. 2022.

825 Downing, J.A. et al: The global abundance and size distribution of lakes, ponds, and
826 impoundments. *Limnol. Oceanogr.*, **51**, 2388-2397. 2006.

827

828 Dutra, E, Stepanenko, V. M, Balsamo, G, Viterbo, P, Miranda, P. M and co-authors: An
829 offline study of the impact of lakes on the performance of the ECMWF surface scheme.
830 *Boreal Env. Res.* 15, 100–112, 2010.

831

832 ECMWF, OpenIFS: Lakes,
833 <https://confluence.ecmwf.int/display/OIFS/3.5+OpenIFS:+Lakes>. Accessed 7 Dec 2021,
834 2020.

835

836 Fiedler, E.K., Martin, M.J., Roberts-Jones, J.: An operational analysis of Lake Surface
837 Water Temperature. *Tellus A*, 6, <https://doi.org/10.3402/tellusa.v66.21247>, 2014.

838

839 Fujisaki-Manome, A., G. E. Mann, E. J. Anderson, P. Y. Chu, L. E. Fitzpatrick, S. G.
840 Benjamin, E. P. James, T. G. Smirnova, C. R. Alexander, and D. M. Wright:
841 Improvements to lake-effect snow forecasts using a one-way air-lake model coupling
842 approach. *J. Hydrometeor.*, **21**, 2813-2828, <https://doi.org/10.1175/JHM-D-20-0079.1>,
843 2020.

844

845 Gao, G., C. Chen, J. Qi, and R. C. Beardsley: An unstructured-grid, finite-volume sea
846 ice model: Development, validation, and application. *J. Geophys.*
847 *Res.*, **116**, C00D04, <https://doi.org/10.1029/2010JC006688>. 2011.

848

849 Gemmill, W., B. Katz, and X. Li: Daily real-time, global sea surface temperature—High-
850 resolution analysis: RTG_SST_HR. NCEP Office Tech. Note 260, 39 pp. Available
851 online at <http://polar.ncep.noaa.gov/mmab/papers/tn260/MMAB260.pdf> , 2007.

852

853 Gu, H., Jin, J., Wu, Y., Ek, M.B., and Subin, Z.M.: Calibration and validation of lake
854 surface temperature simulations with the coupled WRF-lake model. *Climatic Change*,
855 129, 471-483. DOI 10.1007/s10584-013-0978-y, 2015.

856

857 Hamill, T.M.: Benchmarking the raw model-generated background forecast in rapidly
858 updated surface temperature analyses. Part I: Stations. *Mon. Wea. Rev.*, **148**, 689-
859 700. <https://doi.org/10.1175/MWR-D-19-0027.1>, 2020.

860
861 Hostetler, S.W., Bates, G., Giorgi, F.: Interactive coupling of a lake thermal model with
862 a regional climate model. *J. Geophys. Res.*, 98, 5045-5057. DOI:[10.1029/92JD02843](https://doi.org/10.1029/92JD02843),
863 1993.

864 Hunter, T. S., Clites, A. H., Campbell, K. B., & Gronewold, A. D.: Development and
865 application of a monthly hydrometeorological database for the North American Great
866 Lakes - Part I: precipitation, evaporation, runoff, and air temperature. *Journal of Great
867 Lakes Research*, 41(1), 65–77, 2015

868 James, E. P., and S. G. Benjamin: Observation system experiments with the hourly
869 updating Rapid Refresh model using GSI hybrid ensemble-variational data
870 assimilation. *Mon. Wea. Rev.*, **145**(8), 2897-2918. [https://doi.org/10.1175/MWR-D-16-
871 0398.1](https://doi.org/10.1175/MWR-D-16-0398.1), 2017.

872
873 James, E. P., C. R. Alexander, D. C. Dowell, S. S. Weygandt, S. G. Benjamin, G. S.
874 Manikin, J. M. Brown, J. B. Olson, M. Hu, T. G. Smirnova, T. Ladwig, J. S. Kenyon, and
875 D. D. Turner: The High-Resolution Rapid Refresh (HRRR): An hourly updating
876 convection-allowing forecast model. Part II: Forecast performance. *Wea. Forecasting*,
877 150, <https://doi.org/10.1175/WAF-D-21-0130.1>, 2022.

878
879 Kelley, S.G.T, J.G.W. Kelley, and E.J. Anderson: Evaluation of the NASA SPoRT
880 Composite Product of surface water temperatures for large lakes in New England and
881 New York State. *Abstract, 24th Conference on Satellite Meteorology, Oceanography,
882 and Climatology*. Available at
883 <https://ams.confex.com/ams/101ANNUAL/meetingapp.cgi/Paper/381301>, 2021.

884
885 Kourzeneva, E., Martin, E., Batrak, Y., LeMoigne, P. Faroux: Climate data for
886 parameterisation of lakes in Numerical Weather Prediction models, *Tellus A.*, 64: . DOI:
887 [10.3402/tellusa.v64i0.17226](https://doi.org/10.3402/tellusa.v64i0.17226), 2012a.

888
889 Kourzeneva, E., Asensio, H., Martin, E., Faroux: Global gridded dataset of lake
890 coverage and lake depth for use in numerical weather prediction and climate modelling.
891 *Tellus A.*, 64: 15640. [10.3402/tellusa.v64i0.15640](https://doi.org/10.3402/tellusa.v64i0.15640), 2012b.

892
893 Lawrence, D. M., Fisher, R. A., Koven, C. D., Oleson, K. W., Swenson, S. C., Bonan,
894 G., et al.: The Community Land Model version 5: Description of new features,
895 benchmarking, and impact of forcing uncertainty. *Journal of Advances in Modeling Earth
896 Systems*, 11, 4245-4287. <https://doi.org/10.1029/2018MS001583>, 2019.

897
898 Lewis, W. M., Jr.: A revised classification of lakes based on mixing. *Can. J. Fish.
899 Aquat. Sci.* 40, 1779-1787. <https://doi.org/10.1139/f83-207>, 1983

900

901 Mallard, M.S., Nolte, C.G., Spero, T.L., Bullock, O.R., Alapaty, K., Herwehe, J.A., Gula,
 902 J., Bowden, J.H.: Technical challenges and solutions in representing lakes when using
 903 WRF in downscaling applications. *Geosci. Model Dev.*, 8, 1085-1096, 2015.

904

905 Mironov, D., Heise, E., Kourzeneva, E., Ritter, B., Schneider, N., and Terzhevik, A.:
 906 Implementation of the lake parameterisation scheme Flake into numerical weather
 907 prediction model COSMO, *Boreal Environ. Res.*, 15, 218–230, 2010.

908

909 Muñoz-Sabater, J., H. Lawrence, C. Albergel, P. de Rosnay, L. Isaksen, S.
 910 Mecklenburg, Y. Kerr, and M. Drusch: Assimilation of SMOS brightness temperatures in
 911 the ECMWF Integrated Forecasting System. *Quart. J. Roy. Meteor. Soc.*, **145**, 2524–
 912 2548, <https://doi.org/10.1002/QJ.3577> , 2019.

913

914 NASA: Surface water temperature composite.
 915 <https://weather.msfc.nasa.gov/sport/sst/>. Downloaded 2 Nov 2021, 2021

916 National Weather Service: Service Change Notice 20-10. Available at
 917 https://www.weather.gov/media/notification/scn20-10nsst1_0.pdf , 2020.

918 Pondeva, M.S.F.V. de, G.S. Manikin, G. DiMego, S.G. Benjamin, D.F. Parrish, R.J.
 919 Purser, W.-S. Wu, J. Horel, Y. Lin, R.M. Aune, D. Keyser, L. Anderson, B. Colman, G.
 920 Mann, and J. Vavra: The Real-Time Mesoscale Analysis at NOAA’s National Centers
 921 for Environmental Prediction: Current Status and Development. *Wea. Forecasting*, **26**,
 922 593-612. 2011.

923 Powers, J. G., and Coauthors: The Weather Research and Forecasting Model:
 924 Overview, system efforts, and future directions. *Bull. Amer. Meteor. Soc.*, **98**, 1717-
 925 1737, <https://doi.org/10.1175/BAMS-D-15-00308.1>, 2017

926

927 Railsback, B.: Some fundamentals of mineralogy and geochemistry. Figure on lake
 928 salinity at <http://railsback.org/Fundamentals/SFMGLakeSize&Salinity071.pdf>, 2006

929

930 Skamarock, W. C., and Coauthors, 2019: A description of the Advanced Research WRF
 931 version 4. NCAR Tech. Note NCAR/TN-556+STR, 162 pp., [Available online at
 932 http://www2.mmm.ucar.edu/wrf/users/docs/technote/v4_technote.pdf]. 2019.

933

934 Subin, Z. M., Riley, W. J., & Mironov, D.: An improved lake model for climate
 935 simulations: Model structure, evaluation, and sensitivity analyses in CESM1. *Journal of*
 936 *Advances in Modeling Earth Systems*, 4(1). <https://doi.org/10.1029/2011ms000072>,
 937 2012.

938

939 Thiery, W., Stepanenko, V., Fang, X., Jöhnk, D., Li, Z., Martynov, A., Perroud, M.,
 940 Subin, Z., Darchambeau, F., Mironov, D., Van Lipzig, N.: LakeMIP Kivu: evaluating the
 941 representation of a large, deep tropical lake by a set of one-dimensional lake models,

942 *Tellus A: Dynamic Meteorology and Oceanography*, 66:1, 21390, DOI:
943 10.3402/tellusa.v66.21390, 2014.
944

945 U.S. National Ice Center, updated daily: *IMS Daily Northern Hemisphere Snow and Ice*
946 *Analysis at 1 km, 4 km, and 24 km Resolutions, Version 1*. Boulder, Colorado USA.
947 NSIDC: National Snow and Ice Data Center.
948 Doi: <https://doi.org/10.7265/N52R3PMC>. Accessed 8 November 2021, 2021.
949

950 Vanderkelen, I., van Lipzig, N. P. M., Sacks, W. J., Lawrence, D. M., Clark, M.,
951 Mizukami, N., Pokhrel, Y., and Thiery, W.: The impact of global reservoir expansion on
952 the present-day climate, EGU General Assembly 2021, online, 19–30 Apr 2021,
953 EGU21-723, <https://doi.org/10.5194/egusphere-egu21-723>, 2021
954

955 Verpoorter, C., Kutser, T., Seekell, D.A., and Tranvik. L.J.: A global inventory of lakes
956 based on high-resolution satellite imagery. *Geophys. Res. Lett.*, 41, 6396–6402,
957 doi:10.1002/2014GL060641. 2014.
958

959 Wang, F., Ni, G., Riley, W. J., Tang, J., Zhu, D., and Sun, T.: Evaluation of the WRF
960 lake module (v1.0) and its improvements at a deep reservoir, *Geosci. Model Dev.*, 12,
961 2119–2138, <https://doi.org/10.5194/gmd-12-2119-2019>, 2019.
962

963 Weygandt, S. S., S. G. Benjamin, M. Hu, C. R. Alexander, T. G. Smirnova, and E. P.
964 James: Radar reflectivity-based model initialization using specified latent heating
965 (Radar-LHI) within a diabatic digital filter or pre-forecast integration. *Wea. Forecasting*,
966 150, <https://doi.org/10.1175/WAF-D-21-0142.1> , 2022.
967

968 Wilson, R. C., Hook, S. J., Schneider, P., and Schladow, S. G.: Skin and bulk
969 temperature difference at Lake Tahoe: A case study on lake skin effect. *J. Geophys.*
970 *Res. Atmos.*, 118, 10,332-10,346, <https://doi.org/10.1002/jgrd.50786>, 2013.